The FEBS Journal

FEBS PRESS science publishing by scientists

Proton channels in molluscs: A new bivalvian-specific minimal H_V4 channel

Gustavo Chaves[1], Christophe Jardin[1], Arne Franzen[2], Iryna Mahorivska[1], Boris Musset[1,3] and Christian Derst[1]

1 Center of Physiology, Pathophysiology and Biophysics, Paracelsus Medical University, Nuremberg, Germany
2 Institute of Biological Information Processing (IBI-1), Molekular- und Zellphysiologie, Forschungszentrum Jülich, Jülich, Germany
3 Center of Physiology, Pathophysiology and Biophysics, Paracelsus Medical University, Salzburg, Austria

Keywords
Crassostrea gigas; H_V4; minimal proton channel; voltage-gated proton channel type-4; voltage-gated proton channels

Correspondence
G. Chaves, KNMS, Klinikum Nürnberg – Center of Physiology, Pathophysiology and Biophysics, Paracelsus Medical University, Prof. Ernst-Nathan-Str. 1, Nürnberg 90419, Germany
Tel: +49 911 398 6791
E-mail: gustavo.chaves@pmu.ac.at

(Received 7 December 2022, revised 7 February 2023, accepted 13 February 2023)

doi:10.1111/febs.16751

Recently, three proton channels (H_V) have been identified and characterized in *Aplysia californica* (AcH_V1-3). Focusing on AcH_V1 and AcH_V2, analysis of Transcriptome Shotgun Assembly and genomic databases of 91 molluscs identified H_V homologous channels in other molluscs: channels homologous to AcH_V1 and to AcH_V2 were found in 90 species (56 full-length sequences) and in 33 species (18 full-length sequences), respectively. Here, we report the discovery of a fourth distinct proton channel family, H_V4. This new family has high homology to AcH_V1 and AcH_V2 and was identified only in bivalvian molluscs (13 species, 12 full-length sequences). Typically, these channels possess an extracellular S1–S2 loop of intermediate size (~ 20 amino acids) compared to the shorter loops of molluscan H_V1 channels (~ 13 amino acids) and the much larger loops of molluscan H_V2 channels (> 65 amino acids). The characteristic voltage-sensor motif in S4 possesses only two arginine residues with the common third arginine being replaced by a lysine. Moreover, H_V4 channels are much smaller with only around 200 amino acids in total length. The smallest functional channel found so far in nature (189 amino acids) is expressed in the pacific oyster *Crassostrea gigas* (CgH_V4) and might be considered an archetypical minimal proton channel. Functional expression and electrophysiological characterization demonstrated that CgH_V4 shares distinctive hallmarks of other investigated proton channels as high proton selectivity, slow activation, and pH- and voltage-regulated gating. This work is the first description of a H_V4 type channel, adding a new member to the recently expanded family of proton channels.

Abbreviations
Ala (A), alanine; Asn (N), asparagine; Asp (D), aspartate; BIS-TRIS, bis-(2-hydroxyethyl)imino-tris-(hydroxymethyl)-methane; C, cell capacitance; CgH_V4, *Crassostrea gigas* type-4 voltage-gated proton channel; $CH_3SO_3^-$, methanesulfonate; Cl^-, chloride ion; CT, charge transfer centre; EGTA, ethylene glycol-bis(β-aminoethyl ether)-*N*,*N*,*N*′,*N*′-tetraacetic acid; E_H, Nernst potential for protons; GFP, green fluorescent protein; $g_{H,max}$, maximal proton conductance; g_H-*V*, conductance-voltage dependence; Gln (Q), glutamine; Glu (E), glutamate; H^+, protons; HG, hydrophobic gasket; His (H), histidine; H_V, voltage-gated proton channels; H_V1, H_V2, H_V3, H_V4, voltage-gated proton channel type-1, type-2, type-3, type-4, respectively; I_{max}, maximal current at steady state; K3, lysine residue substitution R3 in the VSM of proton channels; Lys (K), lysine; MES, 2-(N-morpholino)ethanesulfonic acid; mizye, *Mizuhopecten yessoensis*; PDB, protein data bank; Phe (F), phenylalanine; pH_i, internal pH; pH_i-sens, internal pH-sensor; pH_o, external pH; pK_a, acid dissociation constant at logarithmic scale; R1, R2, R3, first, second, and third arginine residues of VSM of proton channels, respectively; S.D, standard deviation; SEM, standard error of the mean; S1, S2, S3, and S4, transmembrane segment 1, 2, 3, and 4, respectively; Ser (S), serine; TMA^+, tetramethylammonium; Trp (W), tryptophan; TSA, Transcriptome Shotgun Assembly; *V*, voltage; Val (V), valine; V_{hold}, holding potential; V_{rev}, reversal potential; VSM, voltage-sensor motif; VSP, voltage-sensing phosphatase; V_{thres}, threshold potential; ZB1, ZB2, associated zinc binding site 1 and 2, respectively; ΔpH, difference between external and internal pH; τ_{act}, activation time constant; τ_{deact}, deactivation time constant.

The FEBS Journal **290** (2023) 3436–3447 © 2023 The Authors. *The FEBS Journal* published by John Wiley & Sons Ltd on behalf of Federation of European Biochemical Societies.

Introduction

Proton channels (H_V) are found in many eukaryotic species, from unicellular Alveolata (*Karlodinium*) [1,2] and Haptophytes (*Emiliana*) [3] to multicellular organisms such as plants [4], fungi [5] and Metazoa [6–9]. As such, they are involved in a huge variety of biological functions, from calcification and bioluminescence processes in unicellular organisms [1–3] to sperm maturation [10,11], reactive oxygen species production [12–14] and alveolar pH control in higher animals [15,16]. Most species possess only one gene encoding for a proton channel or completely lack a structural H_V homologue. It was thus a surprise to find three H_V channels in the gastropod *Aplysia californica* (AcH_V1-3) that are all three functional [17]. Whereas AcH_V1 and AcH_V2 are structurally typical proton channels, AcH_V3 has an unusual voltage-sensor motif (VSM) within the fourth transmembrane region (S4), a particularly long extracellular loop between S1 and S2 and a large C-terminal intracellular domain of unknown function. All three channels are proton selective, with AcH_V1 being a regular H_V1 channel, AcH_V2 showing pronounced inward H^+ currents and the atypical AcH_V3 appearing as a proton leaky channel.

In this work, we emphasize on the identification of structural homologues of AcH_V1 and AcH_V2 as typical members of the proton channel family in molluscs. Homologous structures were identified within all four molluscan classes analysed (Bivalvia, Cephalopoda, Gastropoda and Polyplacophora). In Bivalvia a new typical bivalvian-specific proton channel family (molluscan H_V4) was discovered, combining structural features of the other molluscan H_V channel families. We further electrophysiologically characterized the main biophysical properties of an archetypical H_V4 channel of the pacific oyster (*Crassostreas gigas*, CgH_V4) to confirm its functionality.

Results and discussion

Database analysis

Genomic and Transcriptome Shotgun Assembly (TSA) databases of 91 molluscan species were analysed for the presence of typical proton channels according to the recently described *Aplysia* channels AcH_V1 and AcH_V2 [17]. In total, 136 sequences were identified harbouring typical features of proton channels, such as an aspartate as part of the selectivity filter in S1 [18] and a VSM (RxWRxxR) in S4 [19–21]. From these structures 86 channels were found to be full length, 24 channels missed only small parts of the N- and/or C-terminal domains, and 26 partial sequences contained only part of the S1–S4 core segments of the channel. According to their homology, 90 sequences were found to be orthologous to AcH_V1 (molluscan H_V1 family), 33 sequences were orthologous to AcH_V2 (molluscan H_V2 family). In addition, 13 bivalvian sequences were not grouped into these two H_V families as they were clearly paralogous to the AcH_V1 and AcH_V2 channels. Since they clearly do not correspond to the atypical AcH_V3 channel, they were therefore grouped into a fourth bivalvian specific proton channel family within the mollusc kingdom. A complete list of the amino acid sequences and GenBank accession numbers is found in Figs S1–S3. A list of all full-length sequences, under exclusion of highly homologous (> 98%) orthologues from the same genus, is presented in Table S1.

In molluscs, nearly three times the amount of H_V1 orthologues than H_V2 orthologues were identified. This could be explained by an underrepresentation of H_V2 clones in TSA databases due to a lower total expression rate. A closer look at genomic databases however indicates that many species indeed do not have a H_V2 gene. For the pacific oyster *Crassostrea gigas* (GenBank AccNo. NC_047564, [22]) and the eastern oyster *Crassostrea virginica* (GenBank AccNo. NC_035784, [23]) a gene for an H_V1 orthologue was clearly identified (chromosome 6 in *Crassostrea virginica*). In both, the coding region of the respective channel was encoded by two separate exons. An orthologous gene for H_V2, however, was not identified in both genomes.

For a single species, the Yesso scallop (*Mizuhopecten yessoensis*, mizye, [24]), all three channels H_V1, H_V2 and H_V4 and the respective genes were identified in full length. A sequence alignment of these channels can be found in (Fig. 1). A detailed analysis of the genomic localization and organization of the three Yesso scallop H_V genes revealed how the new H_V4 family has evolved. Whereas the gene for mizyeH_V1 possesses only two large exons and was found on scaffold10867 (GenBank Acc.No. NW_018408761/NEDP02004255), the genes for mizyeH_V2 (KP79_PYT14874) and mizyeH_V4 (KP79_PYT14872) were both located on scaffold8507 (GenBank Acc.No. NW_018407582) in close proximity (< 41.000 bp) to each other (Fig. S4). Both genes are separated by a gene of a yet uncharacterized MAM domain-containing protein (KP79_PYT14873). In addition, exon-intron-structure of both genes closely resembles each other: mizyeH_V2 has seven exons, mizyeH_V4 has six exons (Fig. S5). All exon-intron borders of both genes are conserved, only the last exon of the mizyeH_V2 gene is split by an additional intron. As the orientations of the two genes have opposite directions, it can be

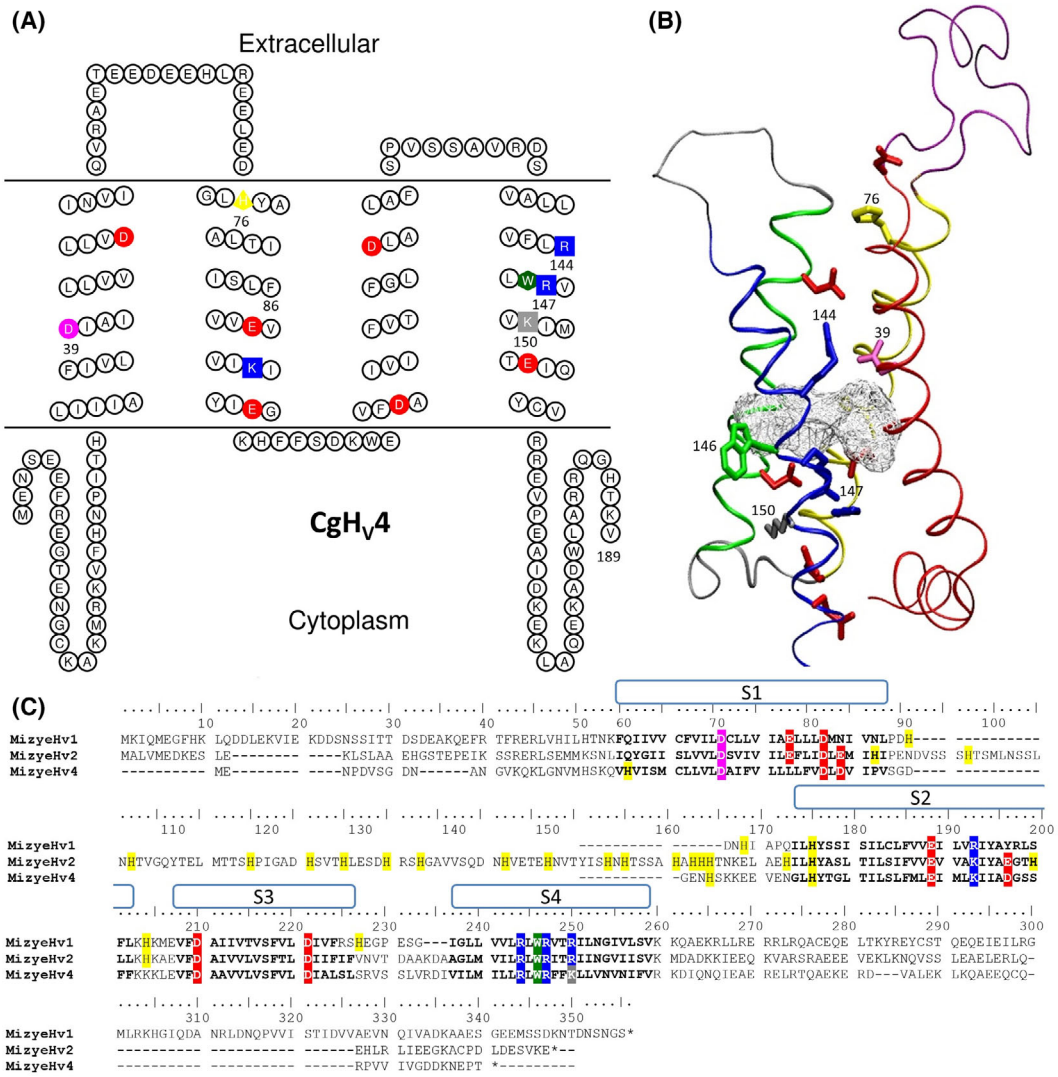

Fig. 1. Bivalvian H_V4 type channel. (A) Amino acids sequence and structural scheme of CgH_V4. A generated scheme using TOPO2 (http://www.sacs.ucsf.edu/cgi-bin/open-topo2.py) shows the sequence of 189 amino acids composing the H_V4 type channel of *Crassosteas gigas*, CgH_V4. Negatively and positively charged amino acids along the transmembrane alpha helices are coloured in red and blue, respectively. The conserved tryptophan and the lysine variation belonging to the characteristic H_V4 VSM, RxWRxxK, are shown in green and grey, respectively. Other functional-related amino acids like the putative selectivity filter (magenta) in S1 and a zinc coordinating histidine (yellow) on top of S2 are also highlighted. (B) Structural model of CgH_V4 in a closed-state. The transmembrane segments are coloured red (S1), yellow (S2), green (S3) and blue (S4). The functional-related and charged amino acids emphasized in (A) are displayed with the same colour pattern. The white-shaded region indicates the position of the HG (guided by Phe^{86}) that separates internal (under) and external (over) vestibules. (C) Full sequences alignment of the bivalvian *Mizuhopecten Yessoensis* H_V1, H_V2, H_V4 channels. Transmembrane segments (S1–S4) are written in bold. The fully conserved Asp residue serving as putative selectivity filter is shown in magenta, His residues along S1–S4 regions are marked in yellow, and Arg residues belonging to the conserved RxWRxxR VSM are presented in blue (Trp in green). The distinctive and special variation Arg to Lys in the VSM of H_V4 channels is shown in grey.

concluded that in a common ancestor of bivalvian molluscs, a gene duplication event with a subsequent inversion of one of the duplicated genes gave rise to two separate H_V2 and H_V4 genes. A phylogenetic analysis supports this evolution of H_V4 channels, as in a dendrogram the H_V4 proteins form a monophyletic group within the H_V2 cluster (Fig. 2).

AcH_V1 and AcH_V2 homologues in Mollusca

The 90 identified AcH_V1 orthologues have all typical structural features of proton channels. Total sequence length varies from 240–280 amino acids in Bivalvia to 350–360 amino acids in most (6/8) Cephalopoda, due to a longer C-terminal domain in the latter class. In Gastropoda, the C-

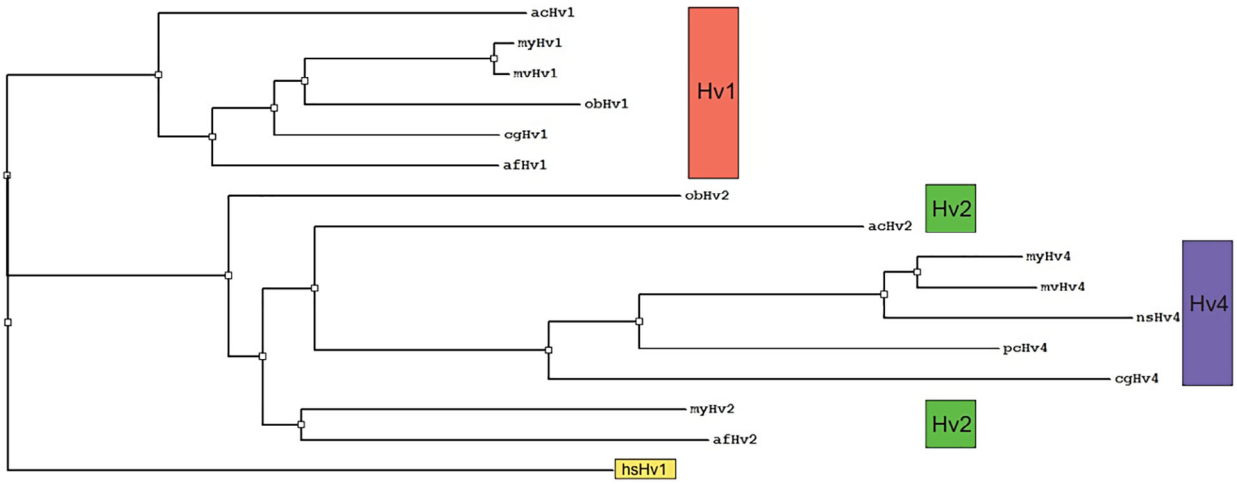

Fig. 2. Phylogenetic tree of basal molluscan proton channels. The different channel families are indicated by coloured bars (H_V1 red, H_V2 green, H_V4 cyan). The human H_V1 channel was selected as outgroup (yellow). Channels were selected from the following molluscan species: ac: *Aplysia californica*, my: *Mizuhopecten yessoensis*, mv: *Mimachlamys varia*, ob: *Octopus bimaculoides*, cg: *Crassostrea gigas*, af: *Acanthochitona fascicularis*, ns: *Nodipecten subnodosus*, pc: *Pomacea canaliculata*.

terminal domain is more flexible in length resulting in proteins of 220–320 amino acids. The only Polyplacophora full-length sequence was found in *Acanthochitona fascicularis* (276 amino acids). Compared to the other molluscan H_V families, the extracellular loop between S1 and S2 is short (~ 13 amino acids), comparable in size to mammalian [25,26] and insect channels [19,20]. A remarkable feature is the conserved length of the N-terminal portion of the channel with a majority of sequences (68%) having a length between 54–57 amino acids.

The 33 identified AcH_V2 orthologues are in total much longer compared to H_V1 and H_V4 channels and sequence lengths vary in a broad range of ~ 300–750 amino acids. An obvious feature of these proton channels is the long extracellular loop between S1 and S2. In Bivalvia, Gastropoda and Polyplacophora the loop is between 65 and 97 amino acids long, in Cephalopoda it is even larger with 118–129 amino acids. With a histidine content of 10–27%, these loops are largely unstructured and may play a role in sensing extracellular pH or zinc binding. For some Cephalopoda, a very long intracellular C-terminal domain (390–470 amino acids) could serve a special but yet unknown function. A list of loop and cytosolic domain lengths of all identified molluscan H_V1-2 channels is presented in Table S1.

A novel bivalvian-specific proton channel family (H_V4)

In bivalvian species, a novel proton channel family was found. With 189–214 amino acids, these channels are the smallest proton channels found so far in Animalia (see Fig. 1 for a sketch drawing and a homology structural model of CgH_V4). Especially the N- and C-terminal domains are of minimal size (~ 30 N-terminal amino acids, 35–50 C-terminal amino acids), whereas the extracellular S1–S2 loop is even a bit larger than for H_V1-type channels (~ 20 amino acids). Interestingly, most of H_V4 S1–S2 loops contain several negatively charged residues (Glu and Asp) that could play a role in coordination of divalent cations involved in inhibition [27–31]; e.g. in *Crassostrea gigas* H_V4 channel, 10 out of 19 residues are negatively charged (Fig. 1). In addition, the length and composition of the S1–S2 loop play a dominant role in the activation kinetics and threshold of activation in fungal H_V1 channels [5]. A comparison of the extracellular loops and the central pore region of H_V1, H_V2 and H_V4 channels is shown in Fig. 3. A list of conserved amino acids in the human hH_V1 and all H_V4 channels identified is shown in Table 1.

Perhaps the most striking structural element characterizing H_V4 channels is in its voltage-sensor. The positively charged voltage-sensor moiety (RxWRxxR) of proton channels is modified as the third arginine (R3) is replaced by a positively charged lysine residue (K3) in all members of this bivalvian H_V4 family, to generate the atypical RxWRxxK pattern.

The presence of an aspartate residue at the middle of the S1 segment, serving as the selectivity filter of proton channels [1,18,19,32] is observed in all H_V4 channels. A notable exception is found in some

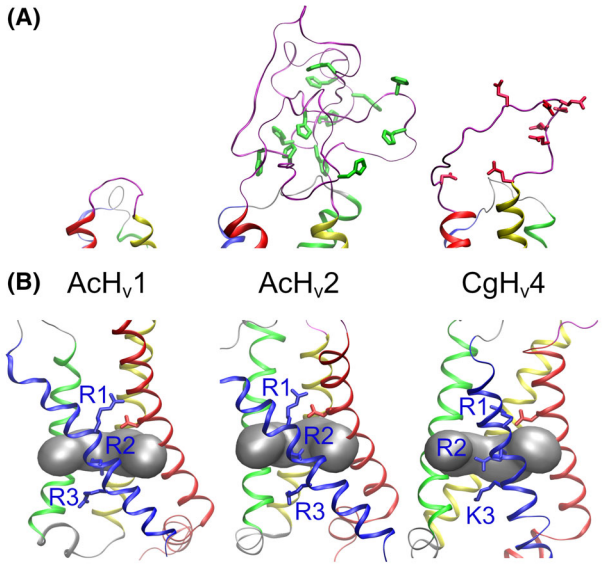

Fig. 3. Structural models of AcH$_V$1, AcH$_V$2 and CgH$_V$4 in putative closed states. (A) The shorter extracellular S1–S2 loop (purple) of AcH$_V$1 has no particular characteristics with regards to the amino acids' composition while that of AcH$_V$2 has a high content of His residues (green sidechains) and that of CgH$_V$4 has a high content of negatively charged amino acids (red sidechains). (B) Views of the transmembrane segments of AcH$_V$1, AcH$_V$2 and CgH$_V$4 showing the characteristic three voltage-sensing arginines, or lysine for K3 in the case of CgH$_V$4, and HG (grey surfaces) that separates the inner and outer vestibules of the proton channels. Colouring scheme of the transmembrane helices S1 to S4 (S1: red, S2: yellow, S3: green and S4: blue).

polyneopteran insects, which possess a negatively charged glutamate residue at this position [20]. The neutralization of the aspartate residue at the specific position in the S1 segment leads to Cl^- permeability in human [18], dinoflagellate [1], and insect proton channels [19].

Zinc has been extensively studied as an inhibitor of H_V channels. The binding of zinc to the structure of H_V1 channels has elicited several interpretations, where both the role of amino acids and the mechanism of inhibition remain debated. Some studies suggest the involvement of negatively charged amino acids in zinc coordination [28,29,31]. However, two main zinc-binding sites each involving one titratable His residue have been identified [26,28–30,33]. The neutralization of both His residues to Ala renders H_V channels zinc-insensitive [26,27,33]. In hH_V1, the first binding site, ZB1, involves position 140 located at the top of the S2 segment. The second binding site, ZB2, comprises position 193 and is found in the S3–S4 loop. The alignment of H_V4 channels (Fig. S6) reveals that all species containing H_V4 exhibit a conserved His residue at the equivalent position in ZB1. However, a variation is observed at ZB2, where all H_V4 channels possess a non-polar aliphatic valine residue instead of a histidine, potentially rendering them less zinc-sensitive compared to mammalian H_V1 channels. The lower zinc sensitivity of the insect channel NpH_V1 has been related to the minor role of the aspartate residue (Asp^{145}) at ZB2, where the main coordination effect is carried by His^{92} at ZB1 [27]. Substituting Asp^{145} to His at ZB2 resulted in increased zinc sensitivity compared to the wild-type channels, similar to mammalian H_V1 [27,34]. The diversity of amino acid residues composing ZB2 is significant among species and H_V variants, while a His residue at ZB1 appears to be a more common structural characteristic for most H_V channels, including the recently discovered H_V4 family.

Other residues are shared by H_V4, H_V1 and H_V2 channels. A tryptophan composing the VSM [21] and a phenylalanine delimiting the charge transfer centre of H_V channels [35–37] are also fully conserved in H_V4. Both residues are considered critical for H_V gating. In humans, Trp^{207} stabilizes the VSM of H_V channels and mutations at this position shift the g_H-V relationship to more hyperpolarized regions [21]. In the case of Phe^{150}, the residue is highly preserved in H_V channels and together with other hydrophobic residues (Val^{109}, Val^{177} and Val^{178}), forms the hydrophobic gasket (HG) of hH_V1 [35]. This hydrophobic region, also called "gating pore", forms a constriction at the centre of the transmembranal segments and is a common element in voltage-activated proteins [38–40]. It is considered to be the focal point of the electrical field and its hydrophobic composition separates the internal and external water vestibules. During gating, gating charge carriers (positive residues of the VSM in S4) move across the HG [35,41,42]. Disruption of the HG in the human H_V1 channel provokes leak of protons at the closed-state which leads to channel's misfunction [35]. Therefore, preservation of Phe residues in this specific position seems to be essential for the proper functioning of H_V channels, and H_V4 fulfils this necessity.

Some negatively charged residues distributed along S1, S2 and S3 segments serving as counter charges are also universal in H_V4 channels (Table 1). In human H_V1, Glu^{153} and Asp^{174} play a crucial role in stabilizing the closed state, while Glu^{119} and Asp^{123} stabilize the open state [43]. The negative residue Asp^{185} opposes V^{116} in closed human H_V1 channels, and Arg^{205} (R1) interacts with it during gating [31]. Notably, Asp^{185} may also be involved in zinc coordination [31]. With the exception of Glu^{119}, which is substituted with aliphatic residues in H_V4 channels, all species have the same residues at the equivalent positions.

Table 1. Comparison of conserved amino acid residues in H_V1 and H_V4 proton channels with functional significance. Basic residues are displayed in blue, acidic residues in red, aromatic residues in green. The conserved aspartate in the middle of S1 responsible for proton selectivity is coloured in magenta. CT, charge transfer centre; pH_i-sens, pH_i sensing; R1-3, VSM charge carriers; SF, selectivity filter; W, VSM tryptophan; ZB1, zinc binding site 1; ZB2, zinc binding site 2. The species designation is represented by letters abbreviations: Ca, *Crassostrea angulata*; Cg, *Crassostrea gigas*; Cv, *Crassostrea virginica*; h, *Homo sapiens*; Me, *Mytilus edulis*; Mv, *Mimachlamys varia*; My, *Mizuhopecten yessoensis*; Ns, *Nodipecten subnodosus*; Pc, *Perna canaliculus*; Pim, *Pinctada margaritifera*; Pir, *Pinctada radiata*; Sb, *Scapharca broughtonii*; Sg, *Saccostrea glomerata*.

Species	SF (S1)	Open-state stabilization (S1/S1/S3)	ZB1 (S2)	CT (S2)	Close-state stabilization (S2/S3)	pH_i-sens (S3)	ZB2 (S3-S4 loop)	R1 (S4)	W (S4)	R2 (S4)	R3 (S4)
hH_V1	D^{112}	E^{119} / D^{123}/ D^{185}	H^{140}	F^{150}	E^{153} / D^{174}	H^{168}	H^{193}	R^{205}	W^{207}	R^{208}	R^{211}
MyH_V4	D^{38}	L^{45} / D^{49} / D^{118}	H^{73}	F^{83}	E^{86} / D^{107}	K^{101}	V^{126}	R^{141}	W^{143}	R^{144}	K^{147}
NsH_V4	D^{38}	L^{45} / D^{49} / D^{118}	H^{73}	F^{83}	E^{86} / D^{107}	K^{101}	V^{126}	R^{141}	W^{143}	R^{144}	K^{147}
SbH_V4	D^{42}	L^{49} / D^{53} / D^{124}	H^{79}	F^{89}	E^{92} / D^{113}	Q^{107}	V^{132}	R^{147}	W^{149}	R^{150}	K^{153}
MvH_V4	D^{38}	L^{45} / D^{49} / D^{118}	H^{73}	F^{83}	E^{86} / D^{107}	K^{101}	V^{126}	R^{141}	W^{143}	R^{144}	K^{147}
PcH_V4	D^{39}	L^{46} / D^{50} / D^{121}	H^{76}	F^{86}	E^{89} / D^{110}	N^{104}	V^{129}	R^{144}	W^{146}	R^{147}	K^{150}
CvH_V4	D^{39}	V^{46} / D^{50} / D^{121}	H^{76}	F^{86}	E^{89} / D^{110}	E^{104}	V^{129}	R^{144}	W^{146}	R^{147}	K^{150}
CgH_V4	**D^{39}**	**V^{46} / D^{50} / D^{121}**	**H^{76}**	**F^{86}**	**E^{89} / D^{110}**	**D^{104}**	**V^{129}**	**R^{144}**	**W^{146}**	**R^{147}**	**K^{150}**
CaH_V4	D^{39}	V^{46} / D^{50} / D^{121}	H^{76}	F^{86}	E^{89} / D^{110}	D^{104}	V^{129}	R^{144}	W^{146}	R^{147}	K^{150}
$PimH_V4$	D^{47}	I^{54} / D^{58} / D^{129}	H^{84}	F^{94}	E^{97} / D^{118}	D^{112}	V^{137}	R^{152}	W^{154}	R^{155}	K^{158}
$PirH_V4$	D^{57}	I^{64} / D^{68} / D^{139}	H^{94}	F^{104}	E^{107} / D^{128}	D^{122}	V^{147}	R^{162}	W^{164}	R^{165}	K^{168}
SgH_V4	D^{38}	V^{45} / D^{49} / D^{120}	H^{75}	F^{85}	E^{88} / D^{109}	D^{103}	V^{128}	R^{143}	W^{145}	R^{146}	K^{149}
MeH_V4	D^{36}	L^{43} / D^{47} / D^{118}	H^{73}	F^{83}	E^{86} / D^{107}	D^{101}	V^{126}	R^{141}	W^{143}	R^{144}	K^{147}

On the other hand, H_V4 channels exhibit a high diversity of residues at the position corresponding to amino acid 168 in hH_V1. This position, located at the bottom of the S3 segment and exposed to the intracellular medium, is occupied by a His residue in hH_V1 that is essential for internal pH-sensing [44]. Mutation of His^{168} to glutamine accelerates activation and deviates ΔpH-gating from the "rule of forty". According to this property, g_H-V relationships shift 40 mV for a 1-unit change in pH_i or pH_o and describe ΔpH-gating for most H_V channels [45]. Interestingly, His residues at this position are common in mammal H_V channels but are swapped with other residues in H_V channels of other species. For example, the H_V channel in the snail *Helisoma trivolvis*, HtH_V1 has a glutamine residue (Gln^{229}) at this position and displays abnormal pH_i sensitivity [46]. In fungi, this position is occupied by amino acids of different physicochemical properties (e.g. Ala, Ser, and Asn). For those fungal channels that were tested, the ΔpH-gating deviated largely from the rule of forty [5]. In H_V4 channels, the species *Scapharca broughtonii* and *Perna canaliculus* have glutamine (Gln^{107}) and asparagine (Asn^{104}) residues, respectively. This raises the possibility that H_V4 channels in those species could have a pH_i sensitivity similar to that of HtH_V1. However, the structural elements regulating pH_i sensitivity in proton channels are most likely more complex, as mutation of Gln^{229} to His in HtH_V1 does not normalize pH_i sensing [46]. Three species, *Mizuhopecten yessoensis*, *Nodipecten subnodosus*, and *Mimachlamys varia*, have a lysine whereas all the remaining species, including *Crossostrea gigas*, have a negatively charged residue. Since the position is exposed to the intracellular solution, it is expected that the pK_a values of these residues are similar to those in bulk solution. Consequently, one would not expect a conventional sensing for little changes of pH_i, as observed in channels with a His at this position.

The smallest H_V4 channel, with only 189 amino acids, was found in the pacific oyster *Crassostrea gigas*. We selected this channel for functional expression and electrophysiological characterization. As a typical proton channel, CgH_V4 possesses a selectivity filter aspartate (Asp^{39}) in the middle of S1, a zinc-binding histidine (His^{76}) at the outer rim of S2 and a totally conserved tryptophan residue (Trp^{136}) within the VSM in S4.

Expression and functional characterization of *Crassostrea gigas* H_V4 channel (CgH_V4)

We used the patch-clamp technique to evaluate CgH_V4 proton channel functionality. To achieve this, GFP-CgH_V4 constructs were transfected into tSA201 or HEK293 cell lines. After 8 h of incubation, CgH_V4 expression was clearly visible in the cell membrane with an expression efficiency of ~ 10% (Fig. 4A). Selected fluorescent cells showed reliable CgH_V4 expression, with a current density of 0.24 ± 0.15 nS/

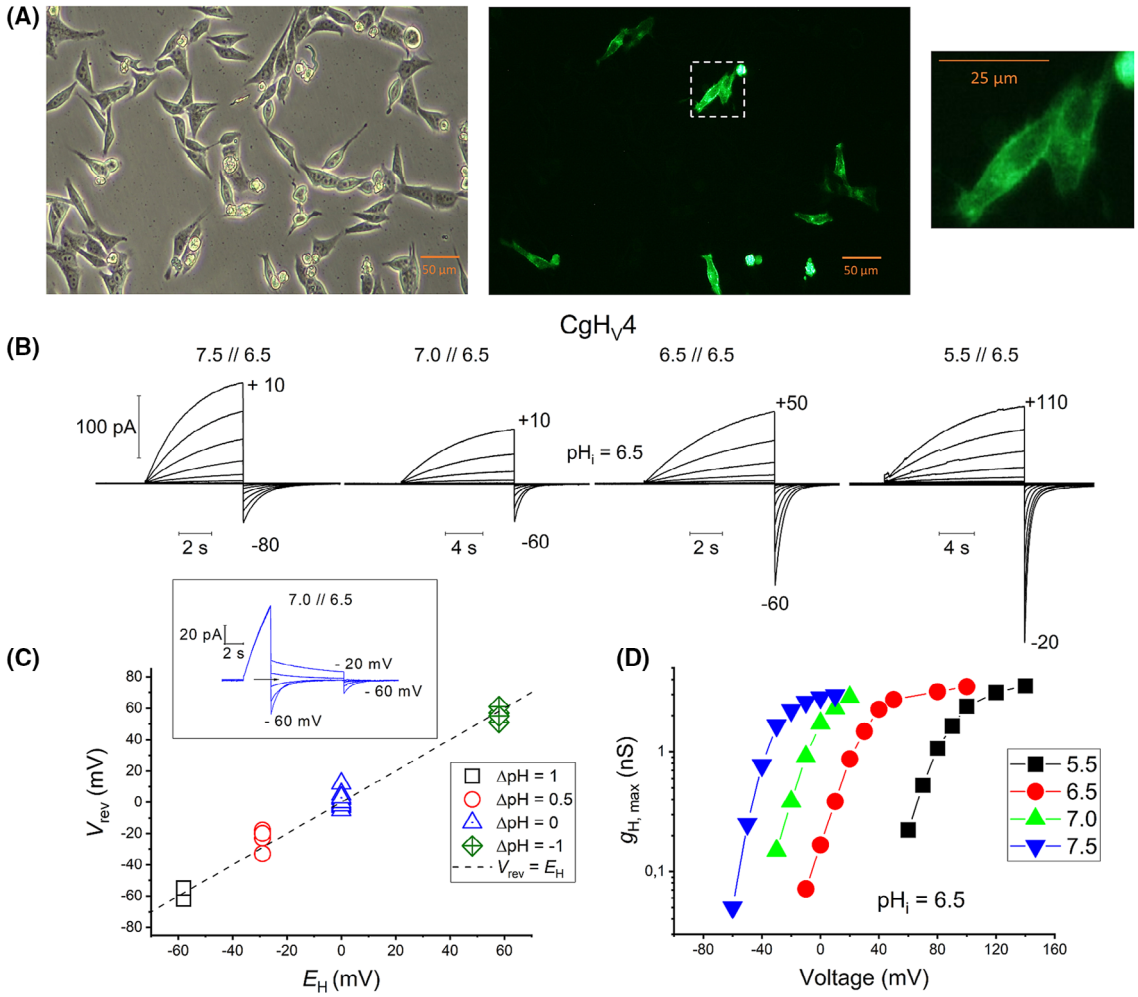

Fig. 4. Expression and functionality of CgH$_V$4. (A) CgH$_V$4 expresses well in the HEK293 cell line. Pictures of the same cell culture taken 8 h after transfection with GFP-CgH$_V$4 plasmid DNA, at 10× magnification (left and central panels). Under fluorescence, expression of CgH$_V$4 is readily distinguished in the cell membrane (central and right panels). A 45× zoom-in of the dashed region of the central photography showing two transfected cells is displayed at the right panel. (B) CgH$_V$4 whole-cell H^+ currents. Families of proton currents for the same cell obtained by *whole-cell* patch-clamp configuration at different pH_o//pH_i as labelled. Depolarization of the cell membrane was done applying pulses in 10 mV increments from the holding potential (V_{hold}) to the positive voltage shown. V_{hold} for pH_o = 7.5, pH_o = 7.0, pH_o = 6.5 and, pH_o = 5.5 were −80 mV, −60 mV, −60 mV and, −20 mV, respectively. The intracellular pH_i was 6.5 for all pH conditions. (C) CgH$_V$4 is a perfect proton selective channel. Measured reversal potentials (V_{rev}) are plotted against the Nernst potential for protons (E_H) at different pH gradients across the membrane (ΔpH). The dotted line represents equality between V_{rev} and E_H and indicates perfect proton selectivity. The inset depicts an example of a V_{rev} determination (arrow; −33 mV) by the tail currents method. Here, test-pulses after a pre-pulse (1 s at +20 mV) were applied in 10 mV increments from −60 to −20 mV, at ΔpH = 0.5. The number of measurements at ΔpH = 1, 0.5, 0, and −1 were 3, 4, 23, and 6, respectively. (D) Voltage- and pH-dependent gating of CgH$_V$4. Maximal H^+ conductance at different pH_o from the proton currents measured in a single cell depicted in B are plotted against voltage.

pF (mean ± S.D.), n = 23 (Fig. S7). Robust sigmoidal H^+ currents conducted through CgH$_V$4 showed clear voltage-dependence of gating typical of H$_V$ channels: currents have threshold of activation (V_{thres}), currents' amplitude increases with depolarization of the cell membrane and show activation time constants (τ_{act}) within seconds (Fig. 4B). Moreover, distinctive H^+ tail currents were observed after repolarization of the cell membrane with deactivation time constants $\tau_{deact} < 1$ s (Fig. 4B).

The selectivity of CgH$_V$4 for protons was evaluated by comparison of measured reversal potentials, V_{rev}, to theoretical values of the Nernst potential for protons, E_H (Fig. 4C). In a wide range of pH_o (5.0–8.0) and pH_i

(5.5–7.5), we measured V_{rev} at different proton gradients. Within our experimental settings, protons are present at concentrations ranging from 10 nM at pH 8.0 to 10 μM at pH 5.0. These concentrations show a clear numerical disadvantage in comparison to other ions, e.g. Cl^-, TMA^+, Mg^{2+}, present at concentrations in the range of 2–90 mM. The difference in concentrations between H^+ and other ions has an important implication. In case of a non-selective channel, the electrochemical driving force and thus V_{rev} would be dominated by the ions of higher concentration in accordance with the Goldman-Hodgkin-Katz equation. During our experiments and in spite of being present in a concentration at least 1000 times lower than other ions, CgH_V4 currents reversed accordingly to E_H for each pH condition tested. Small fluctuations of V_{rev} values away from E_H are associated with poor control of cytosolic pH, e.g. cell H^+ depletion or H^+ accumulation [17,45,47] which are considered common sources of error when measuring proton channels. The conformity of our data with Nernst values for protons allows us to conclude that CgH_V4 is a proton-selective channel.

Furthermore, CgH_V4 currents are also modulated by pH. The pH-dependent gating is a hallmark of proton channels and can be seen as a shift of the conductance-voltage relationship due to changes in ΔpH. Figure 4D depicts an example of a conductance-voltage for CgH_V4. At symmetrical $pH_i//pH_o$ = 6.5, CgH_V4 activates at around −10 mV and its activation shifts rightwards to more positive voltages once pH_o is acidified to 5.5. On the other hand, once the external pH_o is exchanged to more alkaline values (e.g. 7.0 and 7.5), conductance curves shift oppositely to more hyperpolarized regions. At symmetrical pH conditions, the V_{thres} of CgH_V4 is −12 ± 28 mV (mean ± SEM), $n = 23$ (Fig. S7).

For all our data set, the pH-dependent gating of CgH_V4 was determined to be: V_{thres} = 0.84 V_{rev} −12 mV (n = 36), resulting in an approximate change of 49 mV/unit ΔpH in the conductance-voltage relationship (Fig. S7). Interestingly, the pH regulation of the conductance in CgH_V4 is higher than the rule of forty (40 mV/pH) for most of the measured H_V channels [15,45] but is comparable to that of H_V insect channels [19,20]. Compared to other molluscan H_V channels, CgH_V4 shows a pH sensitivity slightly stronger than the molluscan *Aplysia californica* H_V1 and H_V2 channels (~ 45 mV/pH) [17] but still weaker than the anomalously high sensitivity of *Helisoma trivolvis* (60 mV/pH at pH_o 5–7) [46] and fungal channels (80–90 mV/pH) [5]. The similitude of pH-dependent gating of H_V channels from different species is *per se* of interest since it proposes a common mechanism of pH-coupled gating that is still unknown. Further analysis of pH-regulated conductance in other H_V channels and its relationship with common structural features would help to decipher the pH-sensing mechanism of voltage-gated proton channels.

Remarkably, CgH_V4 presents a variation in the gating charges forming the VSM where the third and most internal Arg (Arg^{211} in the human H_V1) is swapped to a Lys (Lys^{150}) to produce the unusual RxWRxxK motif (Fig. 3). Another variation at the voltage sensor motif of H_V channels has also been found in AcH_V3. In AcH_V3, the first Arg of the VSM is replaced by a neutral amino acid (LPWRxxR). The reduced voltage-dependence of gating and the leakage of H^+ at the closed-state were interpreted as potential consequences of this aberration [17]. In sharp contrast, the atypical VSM of CgH_V4 does not impair the gating as drastically as that of AcH_V3. At all voltage ranges tested, no evident H^+ leak currents were detected at the closed-state and g_H-V curves are steep at voltages near to V_{thres} (Fig. 4D).

The pK_a values of arginine and lysine residues in aqueous solution are reported to be ~ 13.8 [48] and 10.4–10.68 [49], respectively. However, values can be significantly altered due to burial into the protein interior, e.g. pK_a values of internal lysine residues in nucleases reported to be as low as 5.3 depending on the polarity of its microenvironment [50]. Studies conducted on proton channels have demonstrated that the arginine residue located at the third position (R3) of the voltage-sensing motif (VSM) is exposed to the cytosolic solution when the channel is in its resting state [42,49,51–55]. Under conditions of negligible pK_a changes due to microenvironmental effects of the CgH_V4 structure on K3, our experimental settings permit protonation of the terminal amino group of Lys^{150}, which would act as a discrete gating charge [56]. Curiously, Lys acting as gating charge carrier in voltage-gated ion channels is not common, as Arg is usually observed in this role. The cause for this prevalence is currently unknown [57]. Additionally, R3K mutations in the human proton channel shift g_H-V relationship to more positive potentials and slow activation kinetics [36]. Further investigations to determine the effect of this natural substitution on CgH_V4 gating would help to clarify the role of Lys as component of the VSM of H_V4 channels.

Conclusion and perspective

With the identification of a H_V4 proton channel family in bivalvians, the diversity of proton channels (in molluscs) is further increased. The smallest naturally occurring H_V4 channel uncovered to date, CgH_V4, appears to be a good candidate to study biophysical

channel functions and to identify minimal structural requirements. In addition, future analysis of structural differences among molluscan proton channels, such as length and charge variations within the S1–S2 loop or the unusual lysine residue at the "R3"-position within the voltage-sensor of H_V4 channels, may help us to understand the unusual expansion within the family of H_V channels in molluscs. It is noteworthy that in addition to possessing tiny H_V channels, molluscs also have the largest known proton channels, the H_V3 family. This indicates a high degree of complexity in terms of structural and functional diversity within these channels.

Materials and methods

Molluscs database analysis

Transcriptome Shotgun Assembly and genomic DNA databases at the National Center for Biotechnology Information (NCBI) were analysed using the BLAST algorithm and the coding sequence of the *Aplysia californica* channels AcH_V1 and AcH_V2 (NCBI reference sequence numbers XM_005100609 and XM_005093050, respectively) as query sequences. Only sequences with significant homology within the S1 and/or S4 segments containing the selectivity filter and voltage sensor were used for further analysis. Genomic sequences were shown using NCBI Sequence Viewer 3.46.1.

Phylogenetic tree

Several molluscan H_V1, H_V2 and H_V4 channels were selected and aligned using ClustalW. As an outgroup the human H_V1 channel (GenBank No. NM_001040107) was chosen. A neighbour phylogenetic tree was created using the ProtDist algorithm implemented in the BioEdit sequence alignment program.

CgH_V4 homology model

A structural model of the CgH_V4 transmembrane domain (amino acids 15–165) was constructed by homology modelling to the transmembrane domain of *Ciona* voltage-sensing phosphatase (VSP) channel (*Ci*-VSP, PDB: 4G80 [58], amino acids 106-244) using MODELLER with the DOPE-based loop modelling protocol for loop refinements (release 10.2; [59]). The best model according to MODELLER's molpdf score was further refined with 3Drefine [60].

Heterologous expression and electrophysiology

The CgH_V4 gene was synthetized and cloned in a pEX-A2 plasmid (Eurofins/Genomics, Ebersberg, Germany). For expression in eukaryotic cell lines, CgH_V4 was subcloned into pQBI25-fC3 using 5′ *Bam*HI and 3′ *Eco*RI restriction sites. A GFP domain was fused N-terminally. HEK293 or tSA201 cell lines at ~ 85% of confluency were transfected with 1 μg of cDNA using polyethylenimine (Sigma, St. Louis, MO, USA). After 12 h at 37 °C in 5% CO_2, cells were trypsinized and replated onto glass coverslips at low density for patch clamp recordings at the same and the next days. For measurements, green fluorescent cells were selected.

Patch-clamp recordings were done as described previously [17,19,20,27]: A patch-clamp amplifier EPC 10 (HEKA, Lambrecht, Germany) was used. Patch pipettes were made from borosilicate capillaries GC 150TF-10 (Harvard Apparatus, Holliston, MA, USA) and pulled using Flaming Brown automatic pipette puller P-1000 (Sutter Instruments, Novato, CA, USA). Pipettes were heat polished to obtain tip resistances from 5 to 9 MΩ once in contact with working solutions. Electrical contact with the pipette solution was achieved by a chlorinated silver wire and connected to the bath with an agar bridge made with Ringer's solution. Seals were formed with Ringer's solution (160 mM NaCl, 4.5 mM KCl, 2 mM $CaCl_2$, 1 mM $MgCl_2$, 5 mM Hepes, pH 7.4) in the bath, and the potential zeroed after the pipette was placed above the cell. Solutions used on whole-cell recordings (pipette and bath) included 100 mM buffer close to its pK_a with tetramethylammonium (TMA^+) and methanesulfonate ($CH_3SO_3^-$) as main ions, 1 mM EGTA, and 1–2 mM Mg^{2+} with an osmolality of 300 mOsm·kg^{-1}. Buffers were HomoPipes at pH 5, 2-(N-morpholino)ethanesulfonic acid (MES) at pH 5.5 and 6.0, Bis-(2-hydroxyethyl)imino-tris-(hydroxymethyl)-methane (BIS-TRIS) at pH 6.5, PIPES at pH 7.0, Hepes at pH 7.5 and Tricine at pH 8.0. Resistance of the seals were > 3 GΩ. Currents are shown without correction for leak or liquid junction potentials. Data were collected between 19 °C and 22 °C. Threshold potentials, V_{thres}, were determined from families of pulses as the potential where the first tail current was observed once the membrane was repolarized. Reversal potentials were measured by two methods. When V_{thres} was negative relative to V_{rev}, it could be readily determined by the zero current. When V_{thres} was positive relative to V_{rev}, it was determined with the tail current method. Overexpression of the channels in small cells resulted in large proton currents which removed enough protons to change pH_i considerably, e.g. due to depletion. Because proton channel gating depends strongly on pH, proton depletion is a significant source of error that must be avoided. To minimize this problem, families with different pulse lengths were applied. Longer pulses were used to determine pulses close to V_{thres} where τ_{act} was slow, while shorter pulses were used at more positive voltages. Recordings were stored on hard discs.

Biophysical characterization of CgH_V4

Proton currents of 23 transfected cells were analysed with Origin (Origin 2017, Northampton, MA, USA). Currents were fitted to a rising exponential to obtain the activation

time constant (τ_{act}) and the maximal proton current (I_{max}). The maximal proton conductance ($g_{H,\ max}$) was calculated from the steady-state current I_{max} (the fitted current extrapolated to infinite time) using reversal potentials (V_{rev}) measured in each solution in each cell. In these fits, the initial delay was ignored and the remaining current usually fitted a single exponential well.

The conductance density of each cell was calculated by dividing the maximum conductance ($g_{H,max}$) by the respective cell capacitance (C). The resulting value was then reported as the arithmetic mean ± standard deviation (S.D), with a sample size of 23 cells.

Selectivity of CgH_V4 for protons was determined by comparison of measured reversal potentials to the Nernst potential for protons (E_H) at the experimental ΔpH ($pH_o - pH_i$). The number of measurements for every pH condition were: $n = 6$ at ΔpH −1; $n = 23$ at ΔpH 0; $n = 4$ at ΔpH 0.5; and $n = 3$ at ΔpH 1.

The threshold of activation at symmetrical pH conditions is reported as the arithmetic mean ± standard error of the mean (SEM), $N = 23$.

The pH dependence of gating was evaluated in a pH range from 5.0 to 8.0 by linear regression of concatenate data from the V_{thres} against V_{rev} plot ($n = 36$, 23 cells), in a potential range from −70 to +70 mV to obtain an equation of the form.

$$V_{thres} = \text{slope } V_{rev} + \text{offset} \quad (1)$$

Acknowledgements

We thank Patricia Romberg for manuscript proofreading. This work was financially supported by Kerscher'sche Stiftung to GC. Open Access funding enabled and organized by Projekt DEAL.

Conflict of interest

The authors declare no conflict of interest.

Author contributions

IM did transfections and kept cell culture. AF cloned DNA. CJ did structural models. CD performed GenBank search, generated phylogenetic tree, analysed data and wrote the manuscript. GC designed and performed patch-clamp experiments, analysed data and wrote the manuscript. BM supervised the project and revised the manuscript. All authors read and approved the manuscript.

Data availability section

The experimental data generated and analysed during this study are included in this article and are available from the corresponding author on reasonable request. The nucleotide sequence data that support the findings are openly available in the European Nucleotide Archive (ENA) at EMBL-EBI at https://www.ebi.ac.uk/ena/browser/view/ using the correspondent GenBank Accession Number shown in supplementary data.

Peer review

The peer review history for this article is available at https://publons.com/publon/10.1111/febs.16751.

References

1 Smith SME, Morgan D, Musset B, Cherny VV, Place AR, Hastings JW & DeCoursey TE (2011) Voltage-gated proton channel in a dinoflagellate. *Proc Natl Acad Sci* **108**, 18162–18167.
2 Rodriguez JD, Haq S, Bachvaroff T, Nowak KF, Nowak SJ, Morgan D, Cherny VV, Sapp MM, Bernstein S, Bolt A *et al.* (2017) Identification of a vacuolar proton channel that triggers the bioluminescent flash in dinoflagellates. *PLoS One* **12**, e0171594.
3 Taylor AR, Chrachri A, Wheeler G, Goddard H & Brownlee C (2011) A voltage-gated H+ channel underlying pH homeostasis in calcifying Coccolithophores. *PLoS Biol* **9**, e1001085.
4 Taylor AR, Brownlee C & Wheeler GL (2012) Proton channels in algae: reasons to be excited. *Trends Plant Sci* **17**, 675–684.
5 Zhao C & Tombola F (2021) Voltage-gated proton channels from fungi highlight role of peripheral regions in channel activation. *Commun Biol* **4**, 261.
6 Thomas RC & Meech RW (1982) Hydrogen ion currents and intracellular pH in depolarized voltage-clamped snail neurones. *Nature* **299**, 826–828.
7 DeCoursey TE (1991) Hydrogen ion currents in rat alveolar epithelial cells. *Biophys J* **60**, 1243–1253.
8 Demaurex N, Grinstein S, Jaconi M, Schlegel W, Lew DP & Krause KH (1993) Proton currents in human granulocytes: regulation by membrane potential and intracellular pH. *J Physiol* **466**, 329–344.
9 DeCoursey TE & Cherny VV (1993) Potential, pH, and arachidonate gate hydrogen ion currents in human neutrophils. *Biophys J* **65**, 1590–1598.
10 Lishko PV, Botchkina IL, Fedorenko A & Kirichok Y (2010) Acid extrusion from human spermatozoa is mediated by flagellar voltage-gated proton channel. *Cell* **140**, 327–337.
11 Zhao R, Kennedy K, de Blas GA, Orta G, Pavarotti MA, Arias RJ, de la Vega-Beltrán JL, Li Q, Dai H, Perozo E *et al.* (2018) Role of human Hv1 channels in sperm capacitation and white blood cell respiratory burst established by a designed peptide inhibitor. *Proc Natl Acad Sci USA* **115**, E11847–E11856.

12 Cherny VV, Henderson LM, Xu W, Thomas LL & DeCoursey TE (2001) Activation of NADPH oxidase-related proton and electron currents in human eosinophils by arachidonic acid. *J Physiol* **535** (Pt 3), 783–794.
13 DeCoursey TE, Morgan D & Cherny VV (2003) The voltage dependence of NADPH oxidase reveals why phagocytes need proton channels. *Nature* **422**, 531–534.
14 Droste A, Chaves G, Stein S, Trzmiel A, Schweizer M, Karl H & Musset B (2021) Zinc accelerates respiratory burst termination in human PMN. *Redox Biol* **47**, 102133.
15 Cherny VV, Markin VS & DeCoursey TE (1995) The voltage-activated hydrogen ion conductance in rat alveolar epithelial cells is determined by the pH gradient. *J Gen Physiol* **105**, 861–896.
16 Murphy R, Cherny VV, Morgan D & DeCoursey TE (2005) Voltage-gated proton channels help regulate pHi in rat alveolar epithelium. *Am J Physiol Lung Cell Mol Physiol* **288**, L398–L408.
17 Chaves G, Ayuyan AG, Cherny VV, Morgan D, Franzen A, Fieber L, Nausch L, Derst C, Mahorivska I, Jardin C *et al.* (2023) Unexpected expansion of the voltage-gated proton channel family. *FEBS J* **290**, 1008–1026.
18 Musset B, Smith SME, Rajan S, Morgan D, Cherny VV & DeCoursey TE (2011) Aspartate 112 is the selectivity filter of the human voltage-gated proton channel. *Nature* **480**, 273–277.
19 Chaves G, Derst C, Franzen A, Mashimo Y, Machida R & Musset B (2016) Identification of an HV1 voltage-gated proton channel in insects. *FEBS J* **283**, 1453–1464.
20 Chaves G, Derst C, Jardin C, Franzen A & Musset B (2022) Voltage-gated proton channels in polyneopteran insects. *FEBS Open Bio* **12**, 523–537.
21 Cherny VV, Morgan D, Musset B, Chaves G, Smith SME & DeCoursey TE (2015) Tryptophan 207 is crucial to the unique properties of the human voltage-gated proton channel, hHV1. *J Gen Physiol* **146**, 343–356.
22 Wang X, Xu W, Wei L, Zhu C, He C, Song H, Cai Z, Yu W, Jiang Q, Li L *et al.* (2019) Nanopore sequencing and De novo assembly of a black-shelled Pacific oyster (*Crassostrea gigas*) genome. *Front Genet* **10**, 1211.
23 Gómez-Chiarri M, Warren WC, Guo X & Proestou D (2015) Developing tools for the study of molluscan immunity: the sequencing of the genome of the eastern oyster, *Crassostrea virginica*. *Fish Shellfish Immunol* **46**, 2–4.
24 Wang S, Zhang J, Jiao W, Li J, Xun X, Sun Y, Guo X, Huan P, Dong B, Zhang L *et al.* (2017) Scallop genome provides insights into evolution of bilaterian karyotype and development. *Nat Ecol Evol* **1**, 120.
25 Sasaki M, Takagi M & Okamura Y (2006) A voltage sensor-domain protein is a voltage-gated proton channel. *Science* **312**, 589–592.
26 Ramsey IS, Moran MM, Chong JA & Clapham DE (2006) A voltage-gated proton-selective channel lacking the pore domain. *Nature* **440**, 1213–1216.
27 Chaves G, Bungert-Plümke S, Franzen A, Mahorivska I & Musset B (2020) Zinc modulation of proton currents in a new voltage-gated proton channel suggests a mechanism of inhibition. *FEBS J* **287**, 4996–5018.
28 Qiu F, Chamberlin A, Watkins BM, Ionescu A, Perez ME, Barro-Soria R, González C, Noskov SY & Larsson HP (2016) Molecular mechanism of Zn2+ inhibition of a voltage-gated proton channel. *Proc Natl Acad Sci USA* **113**, E5962–E5971.
29 Takeshita K, Sakata S, Yamashita E, Fujiwara Y, Kawanabe A, Kurokawa T, Okochi Y, Matsuda M, Narita H, Okamura Y *et al.* (2014) X-ray crystal structure of voltage-gated proton channel. *Nat Struct Mol Biol* **21**, 352–357.
30 Jardin C, Chaves G & Musset B (2020) Assessing structural determinants of Zn2+ binding to human HV1 via multiple MD simulations. *Biophys J* **118**, 1221–1233.
31 Cherny VV, Musset B, Morgan D, Thomas S, Smith SME & DeCoursey TE (2020) Engineered high-affinity zinc binding site reveals gating configurations of a human proton channel. *J Gen Physiol* **152**, e202012664.
32 Dudev T, Musset B, Morgan D, Cherny VV, Smith SME, Mazmanian K, DeCoursey TE & Lim C (2015) Selectivity mechanism of the voltage-gated Proton Channel, H_V1. *Sci Rep* **5**, 10320.
33 Musset B, Smith SME, Rajan S, Cherny VV, Sujai S, Morgan D & DeCoursey TE (2010) Zinc inhibition of monomeric and dimeric proton channels suggests cooperative gating. *J Physiol* **588**, 1435–1449.
34 Cherny VV & DeCoursey TE (1999) pH-dependent inhibition of voltage-gated H(+) currents in rat alveolar epithelial cells by Zn(2+) and other divalent cations. *J Gen Physiol* **114**, 819–838. Erratum in: J Gen Physiol 2004 124(1):103.
35 Bahn R, Cherny VV, Morgan D, Musset B, Thomas S, Kulleperuma K, Smith SME, Pomès R & DeCoursey TE (2019) Hydrophobic gasket mutation produces gating pore currents in closed human voltage-gated proton channels. *Proc Natl Acad Sci USA* **116**, 18951–18961.
36 Wu X, Zhang L & Hong L (2022) The role of Phe150 in human voltage-gated proton channel. *iScience* **25**, 105420.
37 Chamberlin A, Qiu F, Rebolledo S, Wang Y, Noskov SY & Larsson HP (2014) Hydrophobic plug functions as a gate in voltage-gated proton channels. *Proc Natl Acad Sci U S A* **111**, E273–E282.
38 Starace DM & Bezanilla F (2004) A proton pore in a potassium channel voltage sensor reveals a focused electric field. *Nature* **427**, 548–553.
39 Chanda B & Bezanilla F (2008) A common pathway for charge transport through voltage-sensing domains. *Neuron* **57**, 345–351.

40 Islas LD & Sigworth FJ (2001) Electrostatics and the gating pore of shaker potassium channels. *J Gen Physiol* **117**, 69–89.
41 Lacroix JJ, Hyde HC, Campos FV & Bezanilla F (2014) Moving gating charges through the gating pore in a Kv channel voltage sensor. *Proc Natl Acad Sci U S A* **111**, E1950–E1959.
42 Gonzalez C, Rebolledo S, Perez ME & Peter Larsson H (2013) Molecular mechanism of voltage sensing in voltage-gated proton channels. *J Gen Physiol* **141**, 275–285.
43 DeCoursey TE, Morgan D, Musset B & Cherny VV (2016) Insights into the structure and function of HV1 from a meta-analysis of mutation studies. *J Gen Physiol* **148**, 97–118.
44 Cherny VV, Morgan D, Thomas S, Smith SME & DeCoursey TE (2018) Histidine[168] is crucial for ΔpH-dependent gating of the human voltage-gated proton channel, hH_V1. *J Gen Physiol* **150**, 851–862.
45 Decoursey TE (2003) Voltage-gated proton channels and other proton transfer pathways. *Physiol Rev* **83**, 475–579.
46 Thomas S, Cherny VV, Morgan D, Artinian LR, Rehder V, Smith SME & DeCoursey TE (2018) Exotic properties of a voltage-gated proton channel from the snail *Helisoma trivolvis*. *J Gen Physiol* **150**, 835–850.
47 De-la-Rosa V, Suárez-Delgado E, Rangel-Yescas GE & Islas LD (2016) Currents through Hv1 channels deplete protons in their vicinity. *J Gen Physiol* **147**, 127–136.
48 Fitch CA, Platzer G, Okon M, Garcia-Moreno BE & McIntosh LP (2015) Arginine: its pKa value revisited. *Protein Sci* **24**, 752–761.
49 Jardin C, Ohlwein N, Franzen A, Chaves G & Musset B (2022) The pH-dependent gating of the human voltage-gated proton channel from computational simulations. *Phys Chem Chem Phys* **24**, 9964–9977.
50 Isom DG, Castañeda CA, Cannon BR & García-Moreno E. B (2011) Large shifts in pka values of lysine residues buried inside a protein. *Proc Natl Acad Sci USA* **108**, 5260–5265.
51 Boytsov D, Brescia S, Chaves G, Koefler S, Hannesschlaeger C, Siligan C, Goessweiner-Mohr N, Musset B & Pohl P (2023) Trapped pore waters in the open proton channel H_V1. *Small* 2205968.doi: 10.1002/smll.202205968
52 Kulleperuma K, Smith SME, Morgan D, Musset B, Holyoake J, Chakrabarti N, Cherny VV, DeCoursey TE & Pomès R (2013) Construction and validation of a homology model of the human voltage-gated proton channel hH_V1. *J Gen Physiol* **141**, 445–465.
53 Sakata S, Kurokawa T, Nørholm MHH, Takagi M, Okochi Y, von Heijne G & Okamura Y (2019) Functionality of the voltage-gated proton channel truncated in S4. *Proc Natl Acad Sci USA* **107**, 2313–2318.
54 Morgan D, Musset B, Kulleperuma K, Smith SME, Rajan S, Cherny VV, Pomès R & DeCoursey TE (2013) Peregrination of the selectivity filter delineates the pore of the human voltage-gated proton channel hH_V1. *J Gen Physiol* **142**, 625–640.
55 Li Q, Shen R, Treger JS, Wanderling SS, Milewski W, Siwowska K, Bezanilla F & Perozo E (2015) Resting state of the human proton channel dimer in a lipid bilayer. *Proc Natl Acad Sci USA* **112**, E5926–E5935.doi: 10.1073/pnas.1515043112
56 Aggarwal SK & MacKinnon R (1996) Contribution of the S4 segment to gating charge in the shaker K+ channel. *Neuron* **16**, 1169–1177.
57 Armstrong CT, Mason PE, Anderson JLR & Dempsey CE (2016) Arginine side chain interactions and the role of arginine as a gating charge carrier in voltage sensitive ion channels. *Sci Rep* **6**, 21759.
58 Li Q, Wanderling S, Paduch M, Medovoy D, Singharoy A, McGreevy R, Villalba-Galea CA, Hulse RE, Roux B, Schulten K *et al.* (2014) Structural mechanism of voltage-dependent gating in an isolated voltage-sensing domain. *Nat Struct Mol Biol* **21**, 244–252.
59 Sali A & Blundell TL (1993) Comparative protein modelling by satisfaction of spatial restraints. *J Mol Biol* **234**, 779–815.
60 Bhattacharya D & Cheng J (2013) 3Drefine: consistent protein structure refinement by optimizing hydrogen bonding network and atomic-level energy minimization. *Proteins* **81**, 119–131.

Supporting information

Additional supporting information may be found online in the Supporting Information section at the end of the article.

Fig. S1. Amino acid sequences and GenBank accession numbers of H_V1-type molluscan channels.
Fig. S2. Amino acid sequences and GenBank accession numbers of H_V2-type molluscan channels.
Fig. S3. Amino acid sequences and GenBank accession numbers of H_V4-type molluscan channels.
Fig. S4. Gene structure of the *Mizuhopecten yessoensis* scaffold8507.
Fig. S5. *Mizuhopecten Yessoensis* H_V1, H_V2, H_V4 coding exons.
Fig. S6. Multiple sequence alignment of H_V4 and human H_V1 channels' amino acid sequences.
Fig. S7. Statistical analysis of biophysical parameters and evaluation of the pH-dependent gating of CgH_V4.
Table S1. Amino acids length of loops and terminal domains of H_V1, H_V2 and H_V4 orthologs among molluscan species.